Oxid Met (2017) 88:371–382
DOI 10.1007/s11085-017-9720-x

ORIGINAL PAPER

The Effect of Implanted Al and/or Y on the Scale Formation on Low-Al Fe20Cr2Al Alloy

Jerzy Jedlinski[1] · Jean Luc Grosseau Poussard[2] · Jarosław Dabek[1] · Kazimierz Kowalski[3] · Marek Nocun[4] · Grzegorz Smola[1] · Zbigniew Żurek[5]

Received: 27 December 2016 / Published online: 24 January 2017

Abstract The very early stages of the oxidation of an Fe20Cr2Al alloy, unmodified and ion-implanted by aluminium, yttrium and a combination of both elements, Al and Y, were studied at 1100 °C in oxygen using two-stage-oxidation exposures with $^{18}O_2$ as a tracer and subsequent characterisation of the scales using SIMS analyses of distribution of oxygen isotopes and oxide-related negative ion clusters, SEM observations of the surface morphology and photoluminescence spectroscopy analysis of the phase composition. The scales formed in all cases, except for the Al-implanted alloy, exhibited layered structures, with the outer part comprising Fe- and

✉ Jerzy Jedlinski
jedlinsk@agh.edu.pl

Jean Luc Grosseau Poussard
jlgrouss@univ-lr.fr

Jarosław Dabek
dabek@agh.edu.pl

Kazimierz Kowalski
kazimierz.kowalski@agh.edu.pl

Marek Nocun
nocun@agh.edu.pl

Zbigniew Żurek
zzurek@chemia.pk.edu.pl

[1] Department of Physical Chemistry and Modeling of Processes, Faculty of Materials Science and Ceramics, AGH University of Science and Technology, al. Mickiewicza 30, 30-059 Kraków, Poland

[2] LaSIE, Université de La Rochelle, Avenue Michel Crepeau Fermi, 17042 La Rochelle Cedex 01, France

[3] Department of Surface Engineering and Materials Analysis, Faculty of Metals Engineering and Industrial Computer Science, AGH University of Science and Technology, al. Mickiewicza 30, 30-059 Kraków, Poland

Cr-rich oxide, and the inner part being Al_2O_3, which grew due to a mixed outward–inward mechanism . The alumina sub-layers contained the transient oxides and α-Al_2O_3. Implanted Al significantly affected the mechanism of the scale growth, providing that the scale consisted essentially of α-Al_2O_3, and grew via a mixed inward-outward mechanism typical for scales on alumina formers.

Keywords Low-Al FeCrAl alloys · Oxidation mechanism · Ion implantation · Two-stage oxidation

Introduction

Among the currently applied materials, the FeCr-based materials are extensively studied, e.g. [1, 2]. Only some of them, containing sufficient amounts of Al, belong to the group of alumina formers. The research on Fe-xCr-yAl involves mainly: (1) early and late oxidation stages for high-Al alloys, which should lead to either controlled development of the protective α-Al_2O_3 scale or the mitigation of the Al depletion; and (2) optimising the corrosion resistance of low-Al nominally chromia-forming alloys through bulk or surface additions and/or dedicated procedures, including pre-oxidation ones [3–14]. The latter is frequently based on the so-called third-element-effect [15], which although known for many years, is still not fully understood [16].

Previous oxidation studies of the Fe20Cr2Al alloy (composition of alloys given in weight per cent, unless otherwise noted) surface engineered by ion implantation of Al and Y showed that this procedure may result in improved oxidation behaviour [3, 6]. This is illustrated in Fig. 1 by comparing the oxidation kinetic results of non-implanted and Al-implanted Fe20Cr and Fe20Cr2Al alloys. The alloyed Al addition brought about tremendous lowering of the oxidation rate. However, additional surface-applied implanted Al caused a further decrease of the observed weight changes, by factor of about 2. Moreover, the implanted Al-related effect is substantial from the very beginning of the exposure. Hence, whether implanted Al induces the change of the phase composition of the scale or retards the scale growth without altering its composition needs to be investigated.

This query was the major motivation for the research presented in this paper which reports on the effect of ion-implanted additions on the very early stages of scale development during oxidation of the Fe20Cr2Al alloy at 1100 °C. The additions were Al, Y and a combination of Al and Y. Because of the scales were expected to be multi-layered, the efficient, reliable and relatively fast experimental procedure was elaborated and tested towards providing the mechanistic information concerning development of very thin oxide layers having complex structure.

[4] Department of Glass Technology and Amorphous Coatings, Faculty of Materials Science and Ceramics, AGH University of Science and Technology, al. Mickiewicza 30, 30-059 Kraków, Poland

[5] Institute of Inorganic Chemistry and Technology, Cracow University of Technology, ul. Warszawska 24, 31-155 Kraków, Poland

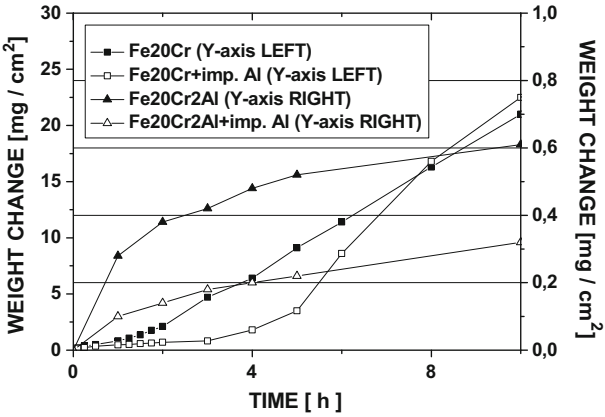

Fig. 1 Oxidation kinetics of non-implanted Al-ion-implanted Fe20Cr and Fe20Cr2Al alloys at 1100 °C in air (partially from [6])

Experimental Procedures

The Fe20Cr2Al alloy was produced by the INCO Ltd. company and made available for research thanks to the courtesy of Prof. W. J. Quadakkers (Forschungszentrum Jülich, Germany). Standard sample preparation procedures were used to make 1-mm-thick discs with a diameter of about 15 mm, and subsequently polished down to 1-μm diamond paste and ultrasonically degreased in acetone.

The following dedicated experimental approach was conceived:

1. ion implantation of aluminium, yttrium and a combination of yttrium and aluminium ions using a beam energy of 70 keV and dose of ions of 2×10^{16} ions/cm^2; the individual specimen was divided into four regions (quarters): non-implanted, implanted with Y, implanted with Al and implanted with (Y+Al). Under such conditions, the penetration depth of implanted additions, estimated according to the LSS-theory [17], should be about 30–50 nm, while the average concentration should be 6–8 at.%, depending on the implanted species and procedure. This information is considered as reliable and sufficient, because of: (1) the close correspondence between the estimation based on LSS-theory and the experimental RBS-profiles obtained for very similar alloys [18]; and (2) the fast formation of scales substantially thicker than the implanted layers during applied oxidation exposures;
2. the two-stage-oxidation experiment at 1373 K, i.e. sequential exposure in $^{16}O_2$ for 2 min. and, subsequently, for 45 s in an $^{18}O_2$-rich atmosphere ($\approx$50 vol% of $^{18}O_2$) with the cold sample quickly inserted into the hot zone of the furnace, pre-heated to the reaction temperature, and with no cooling between the stages (the reacting gas composition was changed through fast pumping away of the first oxidant and filling the reaction chamber with the second oxidant) and rapid cooling down to room temperature by removing it from the high temperature zone after exposure;

3. observations of the scale surface morphology by means of SEM (and EDX for composition analysis, if necessary),
4. determination of the elemental distribution profiles using High-Spatial-Resolution SIMS (HSR-SIMS) with spatial resolution down to approximately 0.3 μm, using the following procedure described elsewhere [19, 20]: (i) analysing the in-depth distribution profiles of negative and positive ions by tracking not only the oxygen isotopes but also the ion clusters related to oxides (negative ions) and the major alloy elements and those applied as implanted surface additions; (ii) special treatment of the oxygen isotopic profiles that resulted in normalised profiles on which is based further interpretation; the raw data obtained for oxygen isotopes were recalculated into so-called normalised in-depth distribution profiles, which corresponded to the 'ideal' atmosphere consisting of the 100 vol% $^{16}O_2$ during the first stage of exposure and 100 vol% $^{18}O_2$ during the second stage of exposure; (iii) careful interpretation of the results, taking into account that the SIMS method does not give quantitative results in terms of elemental concentrations; however, its qualitative outcome might lead to important conclusions after appropriate treatment;
5. the photoluminescence spectroscopy (PLS) using Horiba-Jobin equipment (at La Rochelle University) with lateral resolution of approximately 1 μm was applied to determine and distinguish the alumina phases in the oxide scales. The PLS analytical procedure and interpretation of the PLS spectra, based on the procedure described elsewhere [21] in which the doublets related to Cr^{3+} were detected.

Results

The scale surface morphology (SEM), isotopic in-depth distributions as well as those of negative ion clusters and positive ions (SIMS) and PLS spectra are shown in Figs. 2, 3, 4, 5 for non-implanted, Al-implanted, Y-implanted and (Y+Al)-implanted parts of the sample, respectively. The following should be noted concerning SIMS-results-related plots: (1) in 'E' parts of all figures, the open symbols correspond to the ions associated with the second oxidation stage (in $^{18}O_2$), while the filled one, with the first oxidation stage (in $^{16}O_2$); and (2) the distribution of the $^{16}O^+$ was analysed together with positive metallic ions (parts 'D' in all figures) in order to mark the scale–substrate interface better; and (iii) the normalised in-depth distribution profiles of oxygen isotopes were interpreted as described elsewhere [19, 20, 22].

The following should be pointed out concerning the obtained results:

1. The scale surface morphology consisted of either blocky, well-developed grains, on non-implanted, Y-implanted and (Y+Al)-implanted alloys (Figs. 2, 4, 5, parts A and B), or less-developed fine grains, on Al-implanted alloy (Fig. 3A, B).
2. The normalised in-depth distribution profiles of the oxygen isotopes in the scales indicate a complex (outward + inward) growth mechanism of oxide

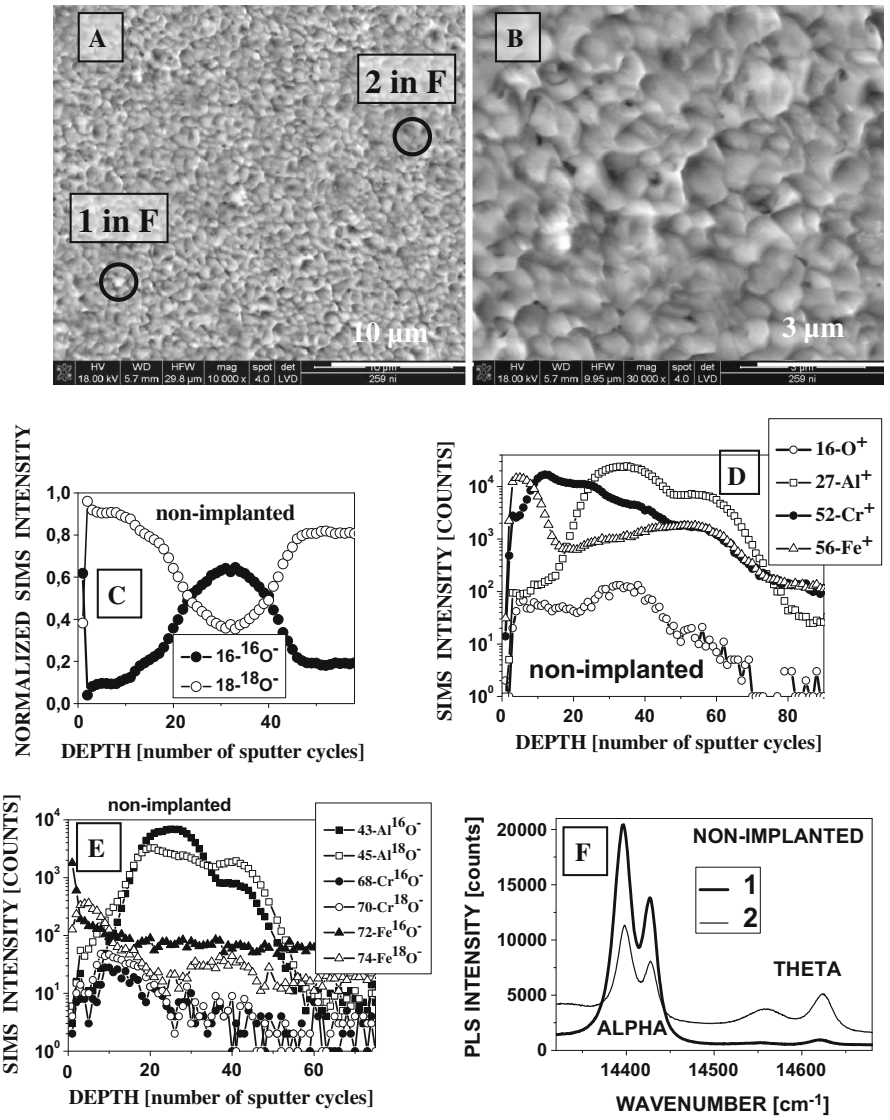

Fig. 2 (**A**, **B**) Surface morphology of the scale formed on non-implanted Fe20Cr2Al alloy oxidised at 1100 °C for 2 min. 45 s. in oxygen (SEM micrographs); (**C**–**E**) SIMS results: normalised distribution of oxygen isotopes (**C**), in-depth distribution profile of positive ions (**D**), in-depth distribution profile of negative oxide-related ion clusters (**E**) and (**F**) the representative photoluminescence spectra (PLS results) (two different regions marked in **A**)

layers formed on all alloys, which is manifested in the $^{18}O^-$ isotope prevailing over the $^{16}O^-$ one at both interfaces—scale-substrate and scale-gas, and opposite relationship in the inner part of the scale (Figs. 2, 3 4, 5, parts C).

3. The distribution of negative ion clusters and positive ions across the scales on non-implanted, Y-implanted and (Y+Al)-implanted alloys (Figs. 2, 4, 5, parts

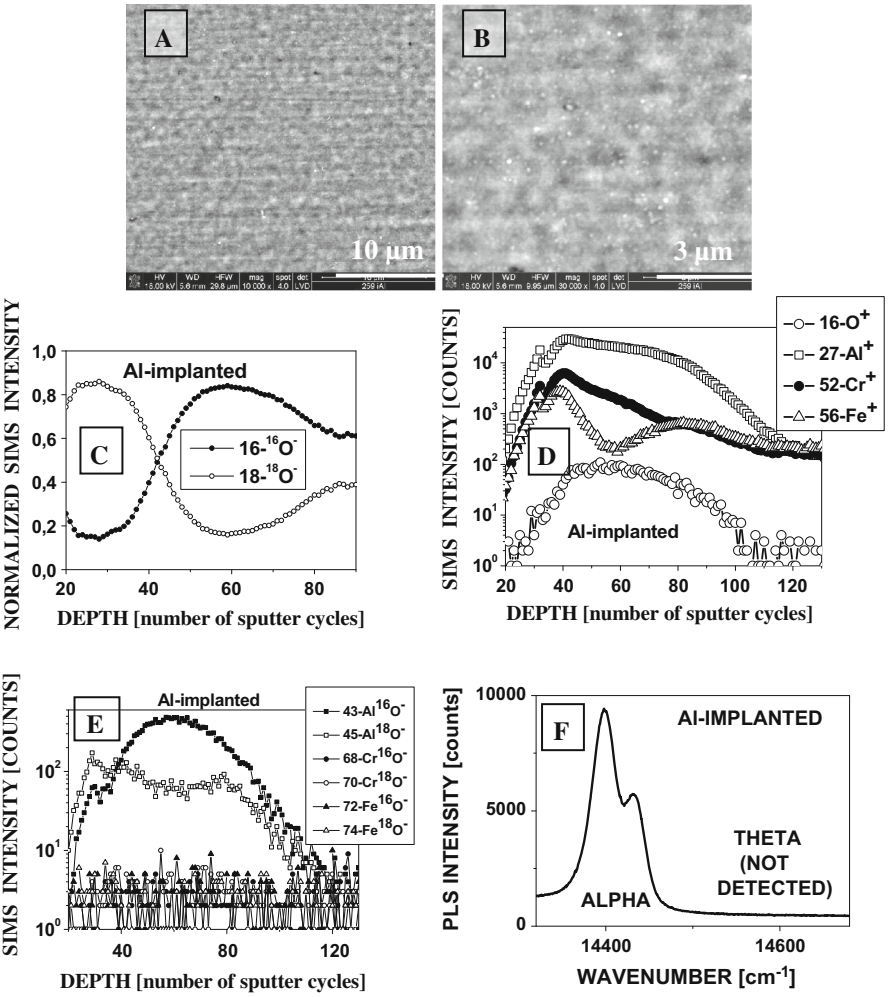

Fig. 3 (**A**, **B**) Surface morphology of the scale formed on Al-implanted Fe20Cr2Al alloy oxidised at 1100 °C for 2 min. 45 s. in oxygen (SEM micrographs); (**C**–**E**) SIMS results: normalised distribution of oxygen isotopes (**C**), in-depth distribution profile of positive ions (**D**), in-depth distribution profile of negative oxide-related ion clusters (**E**) and (**F**) the representative photoluminescence spectrum (PLS results)

D and E) indicate the following: (1) the sequence of oxides comprising Fe-rich, Cr-rich, and Al-rich ones, from the scale-gas to the scale–substrate interface; (2) the internal structure of the distribution of isotopes in alumina, corresponding to the combination of the inward and outward growth mechanisms; (3) the formation of Fe-rich and Cr-rich oxides during the second oxidation stage, as demonstrated by open symbols corresponding to the $(Me^{18}O)^-$ ion clusters (Me = Fe or Cr); (4) non-uniform intensity of $^{16}O^+$ across the scales, which might be associated with different contents of the $^{16}O_2$ in reacting atmospheres during the consecutive exposure stages; 100 vol% during the first stage and $\approx$50 vol%

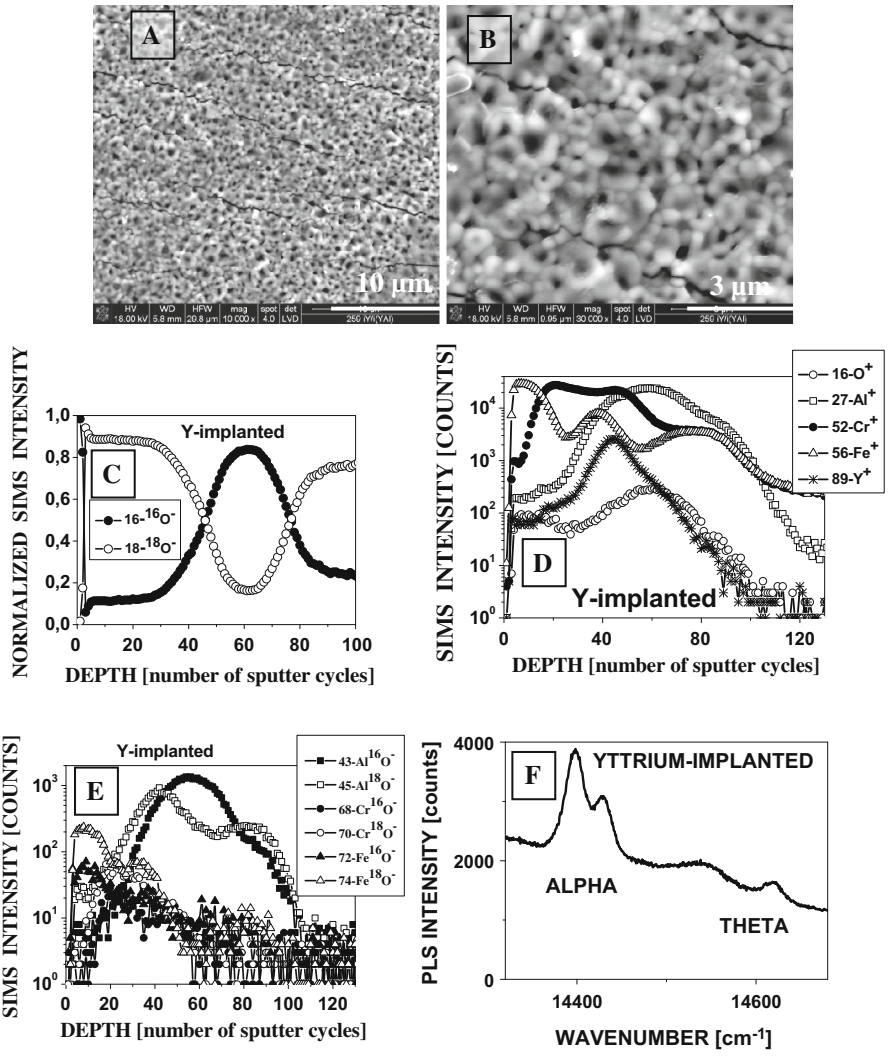

Fig. 4 (**A**, **B**) Surface morphology of the scale formed on Y-implanted Fe20Cr2Al alloy oxidised at 1100 °C for 2 min. 45 s. in oxygen (SEM micrographs); (**C**–**E**) SIMS results: normalised distribution of oxygen isotopes (**C**), in-depth distribution profile of positive ions (**D**), in-depth distribution profile of negative oxide-related ion clusters (**E**) and (**F**) the representative photoluminescence spectrum (PLS results)

during the second stage, and/or with the SIMS analysis-related so-called matrix-effect, relying on the dependence of the yield of secondary ions emission on the target material [23], which manifests itself in different intensities of individual secondary ions sputtered from various oxide sub-layers in the scale; and (5) incorporation of the implanted yttrium into the scales, mainly the alumina sub-layers, and exhibited maximum of its in-depth concentration profiles close to

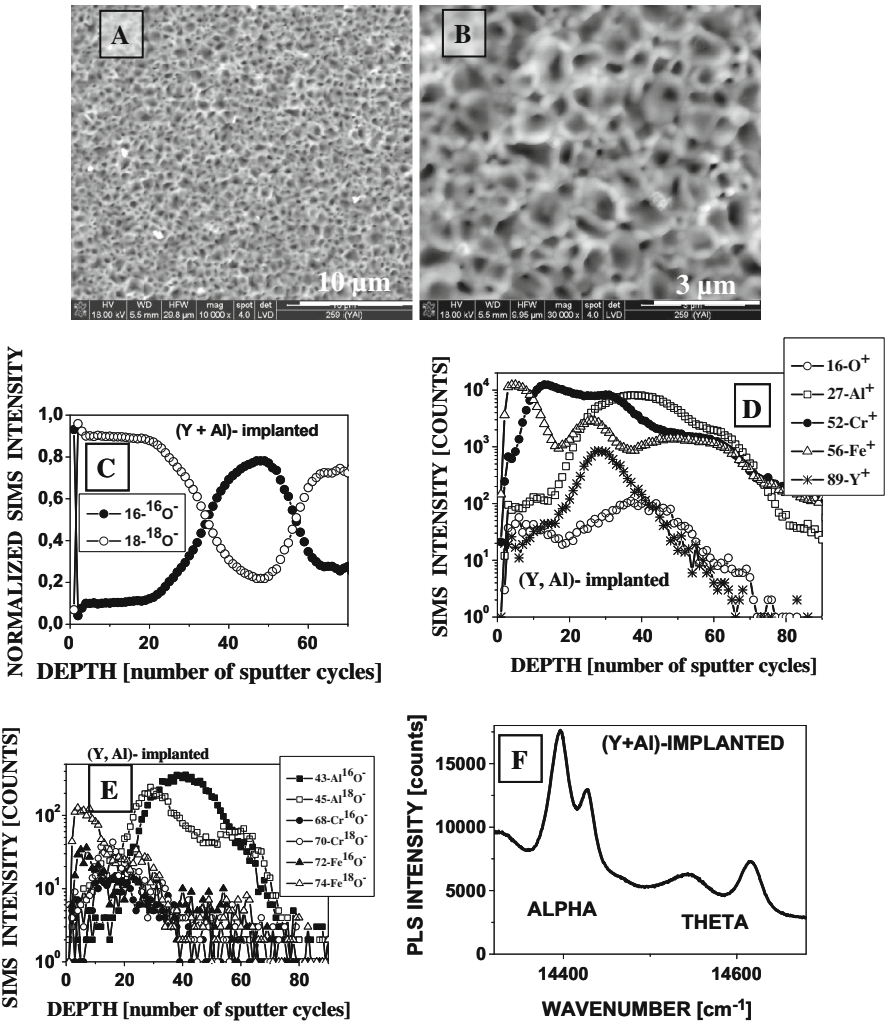

Fig. 5 (**A**, **B**) Surface morphology of the scale formed on (Y+Al)-implanted Fe20Cr2Al alloy oxidised at 1100 °C for 2 min. 45 s. in oxygen (SEM micrographs); (**C**–**E**) SIMS results: normalised distribution of oxygen isotopes (**C**), in-depth distribution profile of positive ions (**D**), in-depth distribution profile of negative oxide-related ion clusters (**E**) and (**F**) the representative photoluminescence spectrum (PLS results)

the interface between the inner alumina sub-layer and the Cr- and Fe-rich top sub-layer.

4. The distribution of negative ion clusters and positive ions across the scales on the Al-implanted alloy (Fig. 3D, E) indicated that: (1) only alumina was present in the scale (no sub-layers of Fe-rich and Cr-rich oxides were found); (2) enrichments in Fe^{3+} and Cr^{3+} ions at the outer part of the scale demonstrated the non-uniform distribution of both elements appearing as dopants in the alumina scale; they might be the remnants of the earlier-formed and already-

disappeared iron oxide and chromia, which should achieve more uniform distribution upon further oxidation.

5. The Cr^{3+} PLS-maxima typical for α-Al_2O_3 were found in scales formed on all alloys (Figs. 2, 3, 4, 5, part F). However, (1) only on the Al-implanted alloy, it was the only aluminium oxide found; (2) in scales formed on yttrium-implanted and (Y+Al)-implanted alloys simultaneously, the Cr^{3+} PLS-maxima typical for θ-Al_2O_3 were also observed (spectra usually consisted of two doublets); and (iii) in scales formed on the non-implanted alloy, two types of spectra were observed—those containing only a doublet related to α-Al_2O_3, and those containing simultaneously both doublets (from α- and θ-Al_2O_3).

Discussion

The obtained results indicate that on all the alloys the alumina was present, but only in the case of Al-implanted alloy did the scale consist essentially of α-Al_2O_3 (parts F of Figs. 2, 3, 4, 5). The scales growing on other alloys exhibited multilayer configurations, and the outermost parts comprised Fe- and Cr-rich oxides, whereas alumina constituted the inner parts, adjacent to the scale–substrate interface. Moreover, usually the alumina contained both: transient polymorphs, represented in photoluminescence spectra by θ-Al_2O_3 and α-Al_2O_3. Thus, the effect of implanted aluminium was twofold: it practically eliminated the formation of Fe- and Cr-containing oxides from the very beginning of oxidation and shortened the period of appearance of transient aluminium oxides. Because all the mentioned oxides grow much faster than α-Al_2O_3, the implanted Al-induced decrease of the oxidation rate begins at very early exposure stages. Early formation of alumina appears to result from the surface enrichment of the substrate in Al caused by the implantation process. Hence, the surface-saturated with aluminium Al-implanted Fe20Cr2Al alloy at initial oxidation stages was converted into strong *alumina former* comparing with bare Fe20Cr2Al alloy. The counter-current growth mechanism—inward + outward—of α-Al_2O_3 scale on Al-implanted Fe-20Cr-2Al alloy is consistent with the reported results obtained for alumina forming FeCrAl alloys that do not contain reactive elements [24–26]. Such a combined mechanism can be associated with the following processes that occur in the scale at grain boundaries of α-Al_2O_3 [27]: (1) inward oxygen transport (inward component) and (2) 'dislocation climbing' towards the scale-gas interface—the mechanism described elsewhere [28] (outward component). It should be noted that in the case of all other alloys, the development of iron and chromium oxides might contribute to the outward growth component, as supported by distribution of the relevant oxide-related ion clusters shown in Figs. 2E ,4E and 5E.

Implanted yttrium did not appear to affect substantially the oxide formation under studied conditions. However, (1) it is known to retard the phase transformation of transient aluminium oxides into α-Al_2O_3, as recently demonstrated for the Fe20Cr2Al alloy from the same manufacturer [24], and (2) no benefits found for the implanted Al were observed for the combined implantation of Al and Y. Therefore,

it is rather clear that yttrium should be considered as the addition that detrimentally affects the possibility of transition from *non-alumina former* to *alumina former* of the low-Al FeCrAl-based alloys, despite its highly beneficial influence on the resistance to spallation of the protective chromia and alumina scales [29–31]. This effect may be attributed to what has been reported elsewhere, e.g. [32, 33]: the tendency of yttrium to tie Al in Y-Al oxides having a perovskite or garnet structure, $YAlO_3$ or $Y_3Al_5O_{12}$, respectively. Thus, yttrium may considerably reduce or even eliminate the efficiency of the implanted Al in fostering the formation of alumina.

Regarding the effect of implanted elements on the phase transformation of transient aluminium oxides (γ-, δ- and/or θ- Al_2O_3) into α-Al_2O_3, it appears that implanted yttrium retarded, while implanted aluminium accelerated this process. However, it should be emphasised that the present study was concerned with the very initial stages of the scale formation, during which the scale significantly evolved and the alloy composition did not provide the exclusive formation of alumina. On the contrary, with the exception of the Al-implanted alloy, alumina constituted only one—the innermost—sub-layer of the scale. Therefore, above-mentioned delayed scale evolution caused by implanted yttrium and accelerated brought about by the implanted aluminium might manifest itself in later or earlier development of α-Al_2O_3, respectively. On the other hand, yttrium was reported to retard the phase transformation by either chemical or mechanical effects, related to doping of transient aluminium oxides, as described elsewhere [30, 34–37]: it may decrease the concentration of defects required for transformation to occur ('chemical effect') or decrease in driving force for the transformation related to enhancement of the strain energy caused by large yttrium cations ('mechanical effect'). All in all, superposition of both effects, on the scale evolution and on phase transformation in alumina, might lead to the observed results, and at present, it is impossible to verify whether any of them was predominant.

It should be noted that: (1) previous research indicates that ion implantation, with the applied parameters (energy, dose) as well as the expected, slightly non-uniform distribution of implanted elements and implantation-induced surface damage of the substrate material, do not noticeably affect the scale development mechanism and, therefore, may be considered as the surface elemental doping tool only [6, 24, 38–40]; (2) cracks in scale observed in Fig. 4 indicate mechanical effects, during cooling from the reaction temperature to the room temperature rather than at the reaction temperature, but they cannot be thoroughly interpreted since such effects were not studied in detail; and (3) only because of the application of the elaborated systematic experimental procedure was it possible to obtain such results.

Conclusions

The obtained results indicate that at very early stages of the oxidation exposure (2 min. 45 s at 1373 K, oxygen):

1. The growth mechanism of the scales on non-modified, yttrium-implanted and (Yttrium + Aluminium)-implanted Fe20Cr2Al alloys is complex. The scales

exhibit the layered structures—the outer part comprising Fe- and Cr-rich oxide, and the inner part being Al_2O_3, which grows due to a mixed outward–inward mechanism. The alumina sub-layer contains the transient oxides and α-Al_2O_3. Implanted yttrium incorporated the scale and was preferentially distributed in alumina, with a maximum close to its outer part at the interface with the outer (Fe+Cr)-rich sub-layer.

2. Implanted Al appears to significantly affect the mechanism of the scale growth by virtue of the effect on its phase composition, providing that the scale consists essentially of α-Al_2O_3. It exhibits a mixed inward-outward growth mechanism, typical for scale on such alumina formers.
3. It should be noted that gaining insight into the scale development process was possible because of the application of a carefully planned comprehensive experimental approach, and taking advantage of the capability of SIMS and PLS analytical techniques. In particular, it is worth noting that important information was obtained by analysing the in-depth distribution profiles of oxide-related ion clusters of $(MeO)^-$-type and of positive ions associated with oxide-forming elements (Me = Fe, Cr and/or Al).

Acknowledgements The financial support from (1) University of La Rochelle and Region Poitou-Charentes, France (partial funding of the research and stay of Jerzy Jedliński), and (2) AGH University of Science and Technology, Poland (Grant No. 11.11.160.768) is gratefully acknowledged.

References

1. M. Schütze, W. J, Quadakkers, J. R. Nicholls, *Lifetime Modelling of High Temperature Corrosion Processes*, European Federation of Corrosion Monograph, Nr. 34, (Maney Publishing, London, 2001).
2. M. J. Bennett, J. R. Nicholls, N. J. Simms, D. Naumenko, W. J. Quadakkers, V. Kochubey, R. Fordham, R. Bachorczyk, D. Goossens, H. Hattendorf, A. B. Smith and D. Britton, *Materials and Corrosion* **56**, 854 (2005).
3. J. Jedlinski, A. Nikiel, G. Borchardt and B. Rajchel, *Materials Science Forum* **163–165**, 449 (1994).
4. F. H. Stott, G. C. Wood and J. Stringer, *Oxidation of Metals* **44**, 113 (1995).
5. J.-M. Herbelin and M. Mantel, *Journal de Physique IV Colloque* **05**, (C7), 365 (1995).
6. J. Jedlinski, G. Borchardt, B. Rajchel and M. Nocun, *Materials Science Forum* **461–464**, 513 (2004).
7. C. C. Tsaur, *High Temperature Oxidation and NaCl-Induced Accelerated Corrosion of Hot-Dip Aluminized 9Cr-1Mo and 310 stainless steel*, Ph.D. Thesis, Texas Agriculture and Mechanical University, College Station, 2004.
8. H. Josefsson, F. Liu, J. E. Svensson, M. Halvarsson and L. G. Johansson, *Materials and Corrosion* **56**, 801 (2005).
9. M. F. Pillis and L. V. Ramanathan, *Surface Engineering* **2006**, (22), 129 (2006).
10. J. Engkvist, U. Bexell, M. Grehk and M. Olsson, *Materials and Corrosion* **60**, 876 (2009).
11. M. H. Bin Ani, T. Kodama, M. Ueda, K. Kawamura and T. Maruyama, *Materials Transactions* **50**, 2656 (2009).
12. M. P. Brady, P. F. Tortorelli, K. L. More and L. R. Walker, *Oxidation of Metals* **74**, 1 (2010).
13. N. Israelsson, *High Temperature Oxidation and Chlorination of FeCrAl Alloys*, Ph.D. Thesis, Chalmers University of Technology, Göteborg, Sweden, 2014.
14. B. A. Pint, K. A. Unocic and K. A. Terrani, *Materials at High Temperatures* **32**, 28 (2015).
15. C. Wagner, *Corrosion Science* **5**, 751 (1965).
16. D. J. Young, *High Temperature Oxidation and Corrosion of Metals*, (Elsevier, Amsterdam, 2008), pp. 338–341.

17. J. Lindhard, M. Scharff and H. Schiott, *Matematisk-fysiske Meddelelser udgivet af Det Kongelige Danske Videnskabernes Selskab* **33**, 1 (1963).
18. W. J. Quadakkers, J. Jedlinski, K. Schmidt, M. Krasovec, G. Borchardt and H. Nickel, *Applied Surface Science* **47**, 261 (1991).
19. J. Jedlinski, *Oxidation of Metals* **39**, 61 (1993).
20. J. Jedlinski, A. Bernasik, K. Kowalski and M. Nocun, *Materials at High Temperatures* **12**, 505 (2005).
21. D. M. Lipkin and D. R. Clarke, *Oxidation of Metals* **45**, 267 (1996).
22. S. N. Basu and J. W. Halloran, *Oxidation of Metals* **27**, 147 (1987).
23. V. R. Deline, W. Katz, C. A. Evans Jr. and P. Williams, *Applied Physics Letters* **33**, 832 (1978).
24. J. Jedliński, J.-L. Grosseau-Poussard, K. Kowalski, J. Dąbek and G. Borchardt, *Oxidation of Metals* **79**, 41 (2013).
25. A. M. Ben Abderrazik, G. Moulin, A. M. Huntz, E. W. A. Young and J. H. W. de Wit, *Soli State Ionics* **22**, 285 (1987).
26. V. K. Tolpygo and D. R. Clarke, *Materials at High Temperatures* **20**, 261 (2003).
27. J. Jedlinski, *Defect and Diffusion Forum* **289–292**, 385 (2009).
28. D. R. Clarke, *Acta Materialia* **51**, 1393 (2003).
29. D. P. Whittle and J. Stringer, *Philosophical Transactions of the Royal Society of London A* **295**, 309 (1980).
30. J. Jedlinski, *Solid State Phenomena* **21, 22**, 335 (1992).
31. S. Chevalier, *Materials and Corrosion* **65**, 109 (2014).
32. K. D. Vernon-Parry, C. R. M. Grovenor, N. Needham and T. English, *Materials Science and Technology* **4**, 461 (1988).
33. R. Cueff, C. T. Nguyen, H. Buscail, E. Caudron, C. Issartel and F. Riffard, *Materials Science Forum* **595–598**, 933 (2008).
34. J. Jedlinski, *Oxidation of Metals* **39**, 61 (1993).
35. J. Jedlinski, *Materials Science Forum* **595–598**, 995 (2008).
36. S. Hayashi and B. Gleeson, *Oxidation of Metals* **71**, 5 (2009).
37. S. Hayashi and B. Gleeson, *Oxidation of Metals* **77**, 237 (2012).
38. J. Jedliński, M. Krasovec, G. Borchardt and J. W. Quadakkers, *Journal de Physique IV* **3**, 591 (1993).
39. J. Jedlinski, G. Smola, K. Kowalski, A. Bernasik, M. Nocun, J. Camra and J. Bonarski, *Materials at High Temperatures* **26**, 259 (2009).
40. J. Jedliński, J. L. Grosseau Poussard, G. Smoła, G. Bonnet, M. Nocuń, K. Kowalski and J. Dąbek, *Materials at High Temperatures* **29**, (2), 59–69 (2012).